Additive Manufacturing 36 (2020) 101645

Contents lists available at ScienceDirect

Additive Manufacturing

journal homepage: www.elsevier.com/locate/addma

Binder jetting additive manufacturing of hydroxyapatite powders: Effects of adhesives on geometrical accuracy and green compressive strength

Zuoxin Zhou [a,d], Alex Lennon [b,d], Fraser Buchanan [b,d], Helen O. McCarthy [c,d], Nicholas Dunne [c,d,e,f,g,h,i,j,k,*]

[a] Centre for Additive Manufacturing, Faculty of Engineering, University of Nottingham, UK
[b] School of Mechanical and Aerospace Engineering, Queen's University Belfast, UK
[c] School of Pharmacy, Queen's University Belfast, Belfast, UK
[d] School of Chemical Sciences, Dublin City University, Dublin 9, Ireland
[e] School of Mechanical and Manufacturing Engineering, Dublin City University, Dublin 9, Ireland
[f] Centre for Medical Engineering Research, School of Mechanical and Manufacturing Engineering, Dublin City University, Dublin 9, Ireland
[g] Department of Mechanical and Manufacturing Engineering, School of Engineering, Trinity College Dublin, Dublin 2, Ireland
[h] Advanced Manufacturing Research Centre (I-Form), School of Mechanical and Manufacturing Engineering, Dublin City University, Glasnevin, Dublin 9, Ireland
[i] Advanced Materials and Bioengineering Research Centre (AMBER), Royal College of Surgeons in Ireland and Trinity College Dublin, Dublin, Ireland
[j] Advanced Processing Technology Research Centre, Dublin City University, Dublin 9, Ireland
[k] Trinity Centre for Biomedical Engineering, Trinity Biomedical Sciences Institute, Trinity College Dublin, Dublin 2, Ireland

ARTICLE INFO

Keywords:
Additive manufacturing
3D printing
Binder jetting
Hydroxyapatite
Polyvinyl alcohol
μ-CT

ABSTRACT

Binder jetting additive manufacturing (AM) is a promising process to print hydroxyapatite (HA) powder into bone tissue implants. However, one challenge remaining is the poor reactivity between HA powder with standard water-based ink. This study investigated different water-soluble adhesives to increase the 3D printability of HA powder. Maltodextrin and polyvinyl alcohol (PVOH) with low and high molecular weight (MW) were blended with HA from 10 to 30 wt%. Powder characterisation and evaluation of the compressive properties and geometrical accuracy of the 3D printed scaffolds were performed to identify the optimal adhesive powder. This study adopted an image registration technique to quantify the geometrical accuracy of the final 3D printed scaffold in a more comprehensive and representative way than conventionally dimensional measurement. With these approaches, a highly promising binder jetting formulation has been developed via mixing HA powder with 30 wt% PVOH (high MW). Samples manufactured from this formulation successfully achieved a geometrical accuracy greater than 85% and an excellent green compressive strength of 5.63 ± 0.27 MPa, which was 500% higher than the commercial binder jetting powder. This is the first study to demonstrate a high level of printability when using a formulation containing ≥ 70 wt% HA powder and a water-based binder in the binder jetting AM process. Using the optimal powder composition developed in this study could potentially improve the structural, mechanical, and biological performances of HA-based 3D scaffolds manufactured using the binder jetting AM process for bone tissue engineering applications.

1. Introduction

Hydroxyapatite (HA) is widely used as bone substitutes as it resembles the chemical composition of the inorganic phase of natural bone. It demonstrates excellent osteoconductivity and can interact with the host bone to form intimate chemical bonds (i.e. osteointegration) [1]. The mechanism of bone healing triggered by HA includes the ability to absorb growth factor – stimulating the healing and the direct effects between HA and osteoblasts to regulate osteoconduction [2–4]. HA has, therefore, been used in clinical applications including implant coating, craniofacial defect repair, and sinus augmentation [5–7].

Recently, additive manufacturing (AM) or three-dimensional printing (3DP) has become a promising tool in the manufacturing of bone substitutes due to design flexibility and great control over the 3D geometries that are fabricated. Among all the AM techniques, binder jetting has a unique ability to fabricate porous implants from a large

* Corresponding author at: School of Pharmacy, Queen's University Belfast, Belfast, UK
E-mail address: nicholas.dunne@dcu.ie (N. Dunne).

https://doi.org/10.1016/j.addma.2020.101645
Received 3 June 2020; Received in revised form 14 September 2020; Accepted 29 September 2020
Available online 2 October 2020

variety of powdered materials at ambient environment [8–11]. It is of particular interest for brittle bioceramic materials that are intrinsically vulnerable to thermally induced residual stress. Binder jetting AM forms solid structures by the interaction between powdered materials and binder liquids selectively deposited onto the powder. Therefore, the identification of an ideal combination of powder and binder formulation is the key to a successful binder jetting process [12–14].

Thermal drop-on-demand cartridges have dominated the commercial binder-jetting AM models (e.g. ColorIet printers from 3D Systems) due to their significantly low cost compared to piezoelectric cartridges. The majority of thermal cartridge failures occurs at the centre of the heating elements due to erosion caused by the inks [15]. Greater reliability is usually achieved via using water-based inks that will not erode the heating element during ink vaporisation [16].

However, HA does not have a high level of reactivity with water. Many studies have attempted to use water-soluble polymeric or ceramic-based adhesives to achieve effective binding with the inert HA [17–21]. A previous study has investigated three different polymers in a water-based binder and subsequently printed each of these binders onto the HA powder bed [22]. The highest compressive strength demonstrated was approx. 4 MPa with 1 wt% polyvinyl alcohol (PVOH) in the binder. However, due to the high volatility of water, the printhead nozzles were routinely blocked by polymer content during the printing process. To overcome this issue, the adhesives were introduced to the powder bed via (i) coating or (ii) blending. Maltodextrin has also been spray coated onto the HA powder during pre-processing [23]. Coating maltodextrin onto the HA powder increased its reactivity with a water-based binder. However, it also increased the particle size of the HA powder, leading to poor printing resolution and accuracy. Therefore, blending the inert powders with an appropriate adhesive represents a potentially better approach. A 3D printed structure of calcium polyphosphate (CPP) demonstrated a compressive strength of approx. 34 MPa when it was blended with 10 wt% PVOH before printing [24]. CPP dissociates to a greater extent in water relative to other salts in the calcium phosphate family, which means it has the highest water solubility as indicated by a solubility product constant of 10^{-15} Ksp [25]. The solubility product constant represents the level at which a solute dissolves in solution. The more soluble a substance is, the higher the Ksp value it has. In contrast, HA demonstrates the lowest water solubility of the calcium phosphate family (i.e. a solubility product constant of 10^{-120} Ksp). Therefore, using a water-based binder with HA during the binder jetting AM process requires a more comprehensive formulation optimisation and investigation. Water-soluble bioceramics have also been investigated to blend with HA powder to improve its reactivity. But they need to be incorporated at a high level of wt% loading to achieve acceptable reactivity, which has a detrimental impact on osteoconductivity, mechanical properties [26] and bioresorption [27]. In a previous study, up to 75% of the $CaSO_4{\cdot}1/2H_2O$ powder was blended with HA powder to achieve sufficient binding strength during the 3DP process [21].

In this study, we propose two potentially promising polymer adhesives (i.e. (i) maltodextrin and (ii) PVOH) to achieve a greater binding strength between the HA powder particles and a higher HA content within the 3D printed scaffold. Maltodextrin is a partially hydrolysed starch that is usually produced with a dextrose equivalent value lower than 20% (i.e. 20% of the reducing power of dextrose), whereas PVOH is synthesised via incomplete hydrolysis of poly(vinyl acetate), resulting in a small number of acetate groups in the polymer chain network [28,29]. Both maltodextrin and PVOH have good biocompatibility and consequently have been used in many biomedical applications, including drug delivery, implants, wound dressing, and contact lens [29,31–33]. This study aimed to develop a HA-based powder formulation for water binder jetting AM manufacturing, which can achieve excellent printability without requiring a high content of the adhesive powder. To the best of the authors' knowledge, this is the first study to investigate the efficiency of different water-soluble adhesives for increasing binder jetting AM printability of HA-based powder formulations. Consequently, the effects of different adhesives and mixing ratios on the key printing properties, e.g. compressive properties and geometrical accuracy compared to the original CAD design, were investigated.

2. Materials and methods

2.1. Powder preparation and characterisation

The HA powder purchased (Capital®, Plasma Biotal Ltd., UK) had a particle size distribution (PSD) of $D_{10} = 45.68\,\mu m$, $D_{50} = 67.84\,\mu m$, and $D_{90} = 94.40\,\mu m$, as measured by laser diffraction analysis using a two laser Sympatec HELOS/BF Particle Sizer Analyser (Sympatec Ltd., UK). The PSD is close to the commercially available binder jetting powders and has been previously reported to result in excellent powder bed packing [20]. The HA powder was blended with one of the following three in-bed binding adhesives: (i) maltodextrin powder (419680, Sigma-Aldrich, UK), (ii) PVOH powder of high molecular weight (MW) (GH-20S, Nippon Gohsei, Japan), and (iii) PVOH powder of low MW (GM-14S, Nippon Gohsei, Japan). According to the manufacturer, both PVOH grades were partially hydrolysed PVOH at a hydrolysis level ranging between 86.5% and 89.0%. Partially hydrolysed PVOH retains a relatively small amount of acetic groups that weaken the inter- and intra-molecular hydrogen bonding of adjacent hydroxyl groups, thus allowing the material to readily dissolved in water [30,34]. Hence, this study only investigated partially hydrolysed PVOH grades as they can achieve high solubility using a water-based binder. The difference in MW of two PVOH powders was inferred by intrinsic viscosity. The manufacturer datasheet indicated the high MW PVOH had a viscosity of 40.0–46.0 mPa s and the low MW PVOH had a viscosity of 23.0–29.0 mPa s. Gel permeation chromatography (GPC) (Agilent 1260 Infinity multidetector GPC system, U.S.A.) was performed to measure the number average molar mass (Mn), mass average molar mass (Mw), and polydispersity index (PDI). Phosphate-buffered saline was used as the solvent media for GPC characterisation.

Before blending, each adhesive powder was milled and sieved to reduce the particle size to the level appropriate for binder jetting AM process. Maltodextrin was milled using a planetary mill (Pulverisette 6, Fritsch, Germany). Each milling cycle was for 2 min at a rotational speed of 300 RPM followed by a 5 min rest, which was repeated five times. A more robust milling procedure was required for PVOH, as it had more resistant particle attrition. The rotational speed was increased to 600 RPM and the milling cycle extended to 5 min followed by a 5 min rest, which was also repeated five times. Post-milling, each powder was sieved through a 90 μm mesh but retained by a 32 μm mesh. Consequently, each adhesive powder demonstrated a similar particle size distribution (i.e. 32–90 μm), which closely matched that of the HA powder. Particle agglomeration was not observed for any of the powders investigated in this study.

Each adhesive powder was blended with the HA powder at a ratio of 10:90 wt%, 20:80 wt%, or 30:70 wt%, with HA being the principal component. Powders were blended using a High-Speed Mixer (Rondol, UK) at a rotational speed of 1600 RPM for 2 min with a 2 min rest – this cycle regime was repeated three times. Previous studies have shown that this protocol results in homogenous powder dispersion [35,36]. The packing of the powder bed at each composition was determined using an approach previously described [20]. A binder jetting AM machine (Zcorp 310, Z Corporation, UK) was used to spread the powder from the feed area to a custom-made reservoir (150 mm × 150 m, with adjustable height) located within the build area. Using this approach, the mass ($m(HA,Adh)$) and height of the powder within the reservoir were measured in order to determine the percentage of *powder bed packing* (Eq. (1)) [20].

$$\textit{Powder bed packing} \quad (\%) = \frac{m(HA,\quad Adh)}{(\%HA \times \rho(HA) + \%Adh \times \rho(Adh)) \times V(reservoir)} \tag{1}$$

where *%HA* and *%Adh* are the weight ratio of HA and adhesive of the powder composition, respectively. ρ represents the density (g cm^{-3}) of HA and adhesive. *V*(*reservoir*) (cm^3) was the volume of the reservoir filled with powder. Droplet penetration behaviour was investigated for each formulation of powder blend using a test protocol previously developed [20]. A standard binder jetting ink containing ≥ 98% water (ZB 7, Z Corporation, UK) was used. A high-speed particle image velocimetry system (LaVision, Germany) was used to record a single droplet of the water-based ink falling from 8 mm above the powder bed and subsequently penetrating it (Fig. 1). The droplet volume was approximately 5 μL. Five replicates were performed for each powder blend. The image velocimetry system was recording at a speed of 60 frames s^{-1}. Droplet penetration time, penetration depth, and wetting ratio were determined. The droplet penetration time was recorded from the time the droplet contacted the powder bed surface and ended when all liquid was drained below the surface [20]. Following granule solidification, the solidified granule was removed from the powder bed. The height and mass were measured and were then used to calculate the penetration depth and wetting ratio [20]. The *wetting ratio* is defined as the volume ratio of powder that has been fully wetted by a single droplet relative to the droplet volume (Eq. (2)).

$$Wettingratio(v/v) = \frac{m(granule) - m(droplet)}{(\%HA \times \rho(HA) + \%Adh \times \rho(Adh)) \times V(droplet)} \quad (2)$$

where *m* (*granule*) and *m* (*droplet*) were mass (g) of the granule and the droplet, respectively. *V* (*droplet*) was the droplet volume (mm^3).

2.2. Binder jetting AM

Two custom-made reservoirs were installed on the feed area and build area of a binder jetting AM machine (Zcorp 310, Z Corporation, UK) to reduce the amount of powder required for the process (Fig. 2). The size of each reservoir was 150 mm × 150 mm with an adjustable height to allow 3D parts to be built within. The standard water-based binder was used, which was a reliable ink for the thermal printhead. During the AM process, the binder droplet was selectively deposited onto the powder bed according to the CAD design. The whole structure was built layer-by-layer at a layer thickness of 100 μm. Two structures were designed and printed: (1) a rectangular porous structure (pore size = 1.2 mm × 1.2 mm) and (2) a cylindrical block structure (Ø6 mm × 12 mm) (Fig. 3). The block scaffold was subsequently used to determine the mechanical properties and the porous scaffold was used to calculate the geometrical accuracy. Post-printing, each scaffold was dried in an oven for 1 h at 70 °C. The drying process was used to remove excessive water binder, which did not interact with the powdered material. Following drying, each block scaffold was de-powdered using compressed air. The handling behaviour and ease to de-powder were observed and a qualitative assessment was conducted between the different 3D printed scaffolds at a function of powder blend formulation.

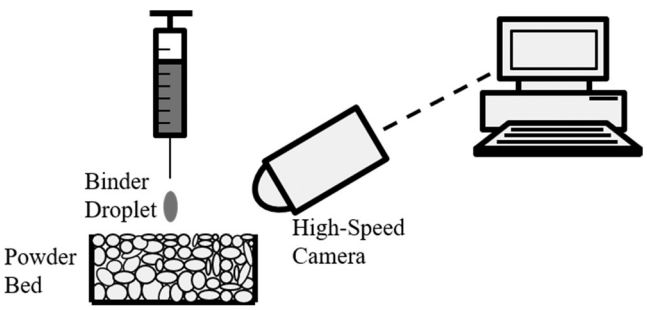

Fig. 1. A schematic diagram of the droplet penetration test setup.

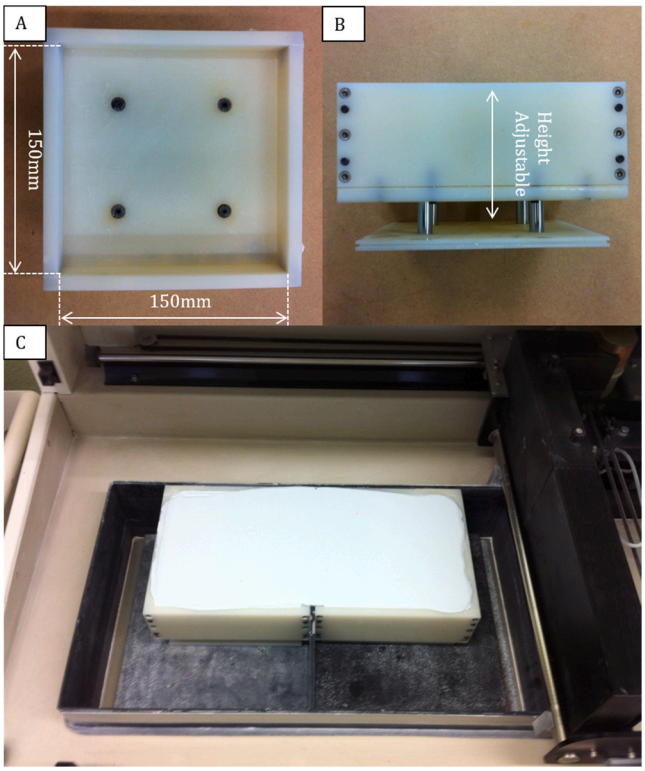

Fig. 2. Custom-made reservoirs to reduce the amount of powder required for binder jetting AM process: (A) top view of the reservoir; (B) side view of the reservoir; and (C) setup of the reservoirs in a binder jetting machine.

2.3. Characterisation

Compression tests were conducted on solid 3D printed scaffolds using a Universal materials test system (EZ50, Lloyds Instruments, UK) with a 5 kN load cell at a rate of displacement of 0.5 mm/min. Each test was completed when the load reduced to 80% of the peak load. The peak load was used to calculate the compressive strength for each specimen. The compressive modulus was determined from the slope of the linear elastic region. Four replicates were performed for each specimen group.

The geometries of porous 3D printed scaffolds were scanned using a SkyScan 1174 compact desktop micro-computed tomography (μ-CT) scanner system (SkyScan N.V., Belgium). Details of the μ-CT scanning process used are described in previously reported studies [9,21]. Reconstruction of the transmission images was performed using SkyScan NRecon software (Version 1.6.3.1), which generated a dataset of cross-sectional images (Fig. 3). To quantify the level of geometrical accuracy, the cross-sectional images from the 3D printed porous scaffold was compared to the reference image from the 3D CAD design. Consequently, a process called image registration was needed to align different images into one coordinate system. The goal of image registration is to map points in one image to the corresponding points in another image [37]. The image that has geometrical transformations is referred to as the target image, while the other image is referred to as the reference image, which remains at a fixed position. The use of image registration is widely adopted across different fields, such as remote sensing, medical imaging, and computer vision [38]. Image registration is an algorithm and the success of this process depends on how well the target and reference images map onto each other. Due to the common information shared by the features in both images, the algorithm can detect points within the target image corresponding to points in the reference image. It then transforms the target image to match the reference image based on point-by-point correspondence [39]. After these two images have been mapped onto each other, a difference image

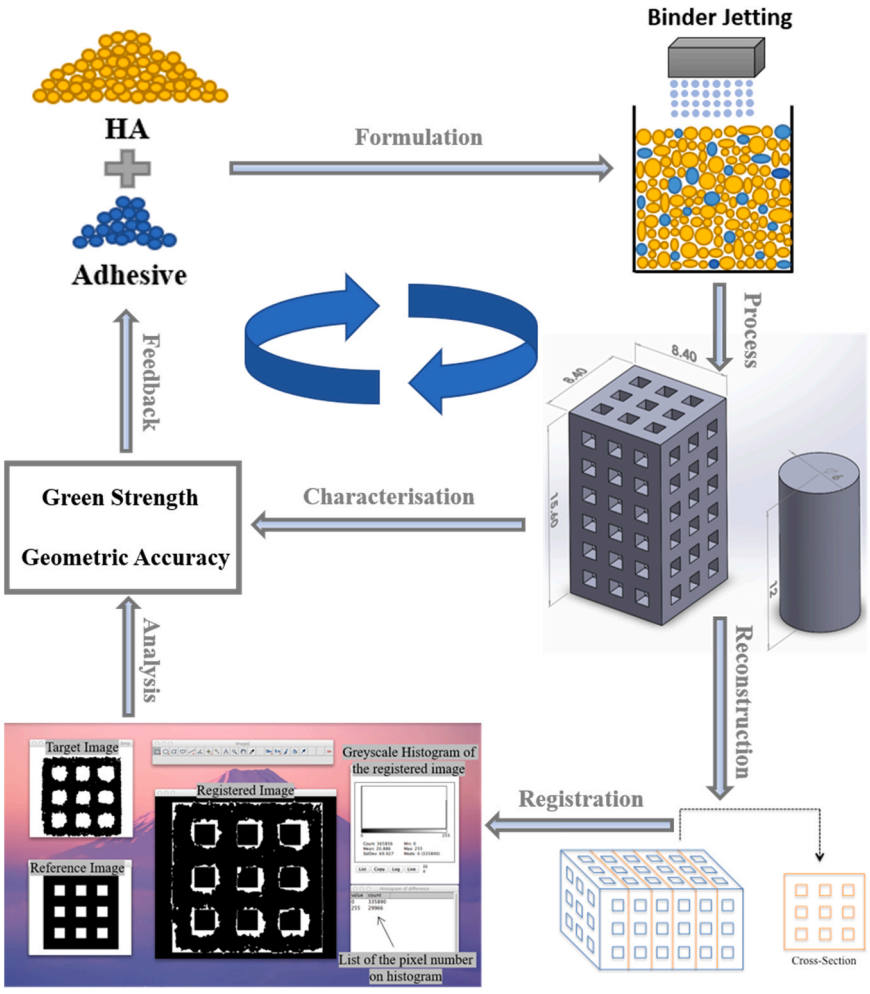

Fig. 3. Schematic diagram showing the overall methodology used in this study. The HA:adhesive powder mixtures were: (i) formulating for binder jetting AM; (ii) processing into solid and porous structures; and (iii) characterised in terms of green strength and geometric accuracy. Geometric accuracy was analysed using ImageJ via image reconstruction and registration. The quality of AM fabricated scaffolds was then feedback to formulation optimisation.

is generated, from which the non-overlapping areas are highlighted. This method facilitates the quantitative measurement of image dissimilarities, and consequently, the geometrical accuracy of the 3D printed porous scaffold.

The reference image was drawn in Solidworks (Dassault Systèmes SolidWorks Corp, U.S.A.) with the same dimensions to the corresponding cross-section of the initial CAD design. Each target image was obtained from the μ-CT dataset following reconstruction. Five cross-sections of each 3D printed porous scaffolds were used as the target images for analysing geometrical accuracy. Their locations were selected to be uniformly distributed across the scaffold geometry (Fig. 3).

Both the reference and target images were imported into ImageJ software (National Institutes of Health, U.S.A.) [40]. Initially, the target image required thresholding as it was in 8-bit format. The 3D printed porous scaffolds fabricated from different powder blend formulations were of varying composition and densities. Therefore for each image, thresholding was performed according to its grayscale histogram. And the threshold level was selected on the cut-off point of an X-ray absorption peak. The reference image did not require thresholding due to its black and white format. Scale set was performed post-thresholding. Each μ-CT image had a pixel size of 16.25 μm, which was used to set the scale. For the reference image, a line was drawn on the bottom boundary and the scale was then set by defining its length as 8400 μm.

Consequently, the two images were registered using an ImageJ plugin program called Rigid Registration [41]. The target image was selected to transform, and the reference image was used as the template. The algorithm was processed under the following setup: n initial positions to attempt = 1; tolerance = 1.000; level = 4; and stop-level = 2. Post-registration completed, a difference image was generated with non-overlapping areas shown in white (grayscale = 255) and overlapping areas shown in black (grayscale = 0) (Fig. 3). The number of pixels that carried either grayscale value was quantified from the histogram of the difference image. Printing accuracy was then calculated by the ratio of the number of black pixels to the number of all pixels (Eq. (3)).

$$Printing\ Accuracy(\%) = black\ pixels/(black\ pixels + white\ pixels) \times 100\% \quad (3)$$

where: *black pixels* and *white pixels* = the number of black and white in the difference image.

2.4. Statistical analysis

The statistical significance of data collected from each experimental test was determined using one-way Analysis of Variance (ANOVA). A post-hoc Tukey' HSD test was performed. A p-value < 0.05 denoted significant difference between two compared sample groups.

3. Results

3.1. Powder characterisation

The two PVOH grades investigated in this study had similar hydrolysed levels (86.5–89%) and only differed in their M_W. GPC indicated the PVOH (low MW) and PVOH (high MW) was M_n of 70,130 and 227,860, respectively (Table 1). M_n and M_w represent the number average molecular weight and weight average molecular weight and relate to determining the molecular mass of a polymer. M_n is defined as the total weight of polymer divided by the total number of molecules. Whereas, M_w depends not only on the number of molecules present, but also on the weight of each molecule [42]. The PVOH (high MW) demonstrated a more heterogeneous molecular size distribution resulting in a higher PDI and greater M_w than PVOH (low MW). GPC indicated the PVOH (high MW) grade showed a greater proportion of larger molecules, which made it more distinct when compared to PVOH (low MW). The maltodextrin powder demonstrated similar molecular weight distribution to PVOH (high MW). These two polymer-based adhesives showed a 4.34% and 6.70% difference in M_w and PDI. The characteristics of the adhesives investigated ensured rational comparisons could be made between the: (i) PVOH of different MW; (ii) PVOH and maltodextrin; and (iii) same composition at different mixing ratio with HA powder.

The interaction between water-based ink droplets and HA powder bed containing each adhesive at different ratios was studied. The results may help interpret the quality of printed structures for each powder blend composition. All powders exhibited a relatively short droplet penetration time with the highest being 376 ± 88 ms for a powder bed containing 10 wt% PVOH (high MW) (Fig. 4). On average, ink droplets were able to penetrate the rest of the powder bed within 300 ms. Powder bed containing maltodextrin demonstrated a wetting ratio over four times greater to than those containing PVOH (p-value < 0.05). The HA: maltodextrin powder blend formed from a single droplet also exhibited significantly greater depth (3.94 ± 0.29 mm), when compared to PVOH: maltodextrin powder at the same adhesive ratio (2.54 ± 0.18 mm and 2.65 ± 0.26 mm) (p-value < 0.05). Overall, PVOH at a lower ratio resulted in a higher wetting ratio and greater droplet penetration depth. There was no significant difference between different PVOH grades at the same ratio (p-value > 0.05) with the only exception being the wetting ratio when 20 wt% PVOH was used. There was no significant difference in the powder bed packing between the investigated powder compositions (p-value > 0.5). Packing values ranged between 36% and 40%, which was similar to the packing ratios for a similar grade of HA powder [20]. It has been discussed that the particle size distribution was the main factor contributing to the powder bed packing. [20] The powder particle size used in this study was within the ideal range for the HA and adhesive powders. Therefore, the spreadability required to fill the powder bed was consistent for all powder compositions investigated in this study.

3.2. Binder jetting AM process

Three powder blend formulations resulted in insufficient handling properties for the porous 3D printed scaffolds from those powders, i.e. (1) 10 wt% maltodextrin in HA; (2) 20 wt% maltodextrin in HA; and (3) 10 wt% PVOH (low MW) in HA. Therefore, these compositions were not considered to be candidate powder blends warranting further investigation. Amongst the remaining six powder blend formulations, 30 wt% maltodextrin demonstrated a de-powdering issue. Specifically, a needle was used to remove a portion of the residual powder from within the pores and then the structure was de-powdered using compressed air (Fig. 5). The same situation did not occur when the HA:PVOH powder blends were used, irrespective of the PVOH grade or compositional ratio. All the residual HA:PVOH powder from within the porous scaffold post-fabrication was easily removed using compressed air.

Table 1
Characteristics of the three adhesive powders investigated.

	Hydrolysed Level (%)[a]	Viscosity (mPa s)[a]	M_n (g mol^{-1})	M_w (g mol^{-1})	PDI
PVOH (low MW)	86.5–89	23.0–29.0	22,480	70,130	3.12
PVOH (high MW)	86.5–89	40.0–46.0	38,950	227,860	5.85
Maltodextrin	N/A	N/A	34,760	217,950	6.27

[a] Denoted properties provided by the manufacturer.

3.3. Geometrical accuracy

The μ-CT scanning images of 3D printed scaffolds demonstrated their internal porous structure. By overlapping the μ-CT images with the original CAD design, the geometrical accuracy of the porous scaffolds fabricated from the different powder compositions was then determined (Fig. 6). The HA:maltodextrin structure exhibited two significant issues: (i) the overall structure was highly distorted; and (ii) the pores had irregular shapes of heterogeneous dimension. Conversely, the majority of the HA:PVOH (irrespective of MW) 3D printed scaffolds demonstrated greater accuracy in terms of overall shapes and pore structures. Pores were close to the square shape and only slightly larger when compared to the initial CAD design. For the 3D printed scaffold containing 20 wt% PVOH (low MW), significant cracking was observed at the edge of the scaffold, which resulted in inferior mechanical integrity. However, further reduction in the adhesive ratio to 10 wt% resulted in insufficient handling properties post-processing. Poor mechanical integrity was not observed for the 3D printed scaffolds fabricated using the HA:PVOH (high MW) powder blends irrespective of compositional ratio. A mildly incomplete structure was observed at one of the vertices of the 3D printed porous scaffolds fabricated from the 90:10 wt% HA:PVOH (high MW) powder blend.

Using the μ-CT scanning images, quantification of the geometrical accuracy was conducted. At 30 wt%, the 3D printed porous scaffolds using maltodextrin as the adhesive demonstrated significantly lower geometrical accuracy (p-value < 0.05) when compared to the PVOH equivalent (Fig. 7). The scaffold fabricated using HA:maltodextrin exhibited a geometrical accuracy of 78.82 ± 1.43%, suggesting a mismatching between the fabricated scaffold and the initial CAD design of approx. 21%. The only HA:PVOH powder blend that resulted in a scaffold of relatively poor geometrical accuracy was 20 wt% PVOH (low MW) and internal cracking within its microstructure. Higher levels of geometrical accuracy were achieved for 3D printed scaffolds fabricated with a greater level of PVOH. At 30 wt%, the HA:PVOH (high MW) scaffold exhibited 85.68 ± 1.19% geometrical accuracy and the HA: PVOH (low MW) structure exhibited 84.60 ± 0.68%. Comparing the quantified data with the cross-sectional images, it was observed the mismatch in geometrical accuracy between the initial CAD design and the final 3D printed scaffold was largely due to over-size in the pores.

3.4. Compressive properties

The green compressive properties are important because they demonstrate how well the 3D printed scaffold can maintain its geometrical integrity during post-processing when subjected to external forces (e.g. compressed air during the de-powdering process). For all powder blend formulations investigated, the 3D printed structures fabricated using the powder containing 30 wt% PVOH (high MW) demonstrated the highest compressive strength (5.63 ± 0.27 MPa) (Fig. 8). It was significantly higher (p-value < 0.05) when compared to the same structure fabricated from HA:maltodextrin (3.70 ± 0.47 MPa) and HA:PVOH (low MW) (0.37 ± 0.01 MPa) at the same ratio. As the ratio of PVOH (high MW) decreased to 20 wt% and 10 wt%, the compressive strength decreased significantly to 2.31 ± 0.11 MPa and 1.15 ± 0.16 MPa (p-value < 0.05). The 3D printed scaffolds fabricated

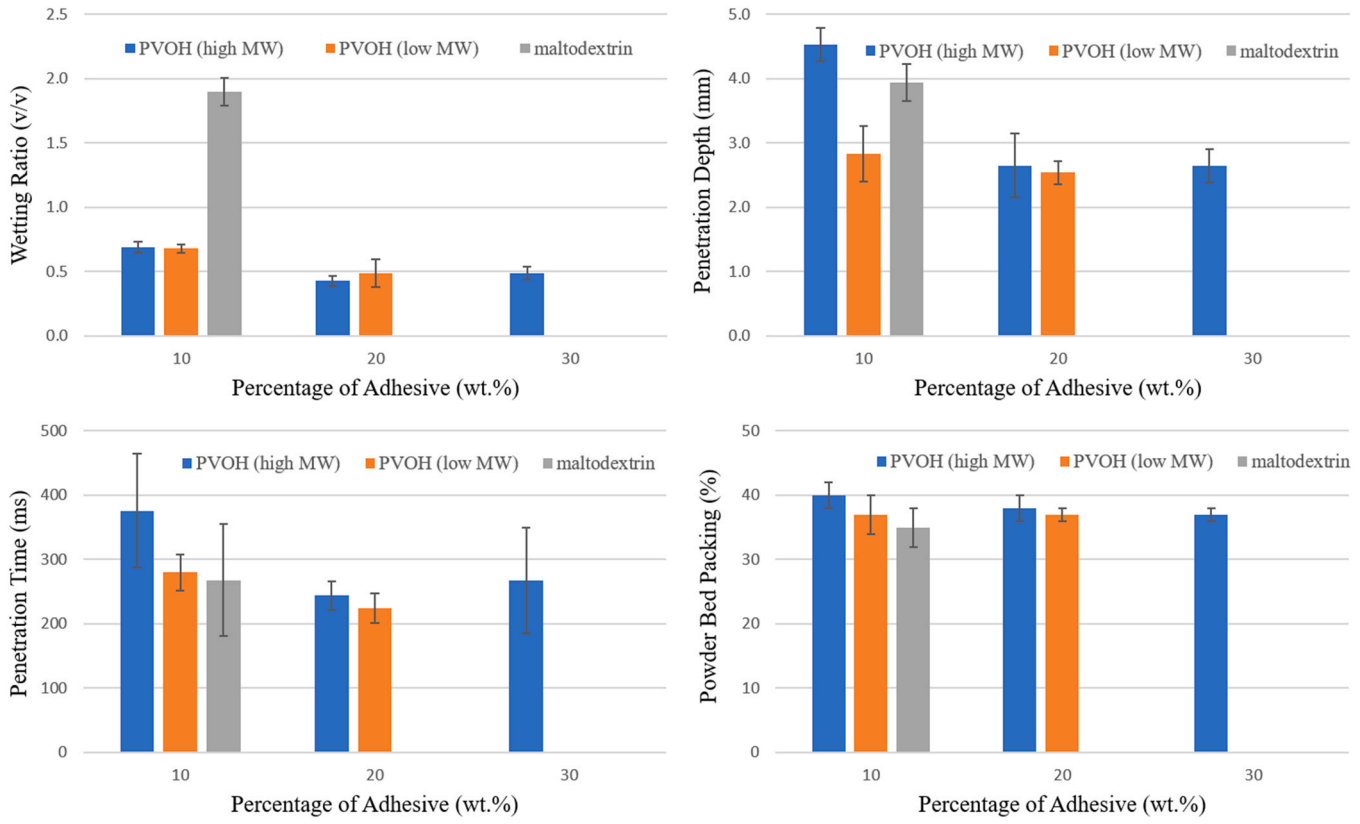

Fig. 4. Wetting ratio, droplet penetration time, penetration depth, and powder bed packing of HA:adhesive powder blend formulations at different adhesives and mixing ratios. Maltodextrin at 10 wt%, 20 wt% and PVOH (low MW) at 10 wt% were not investigated due to insufficient handling properties.

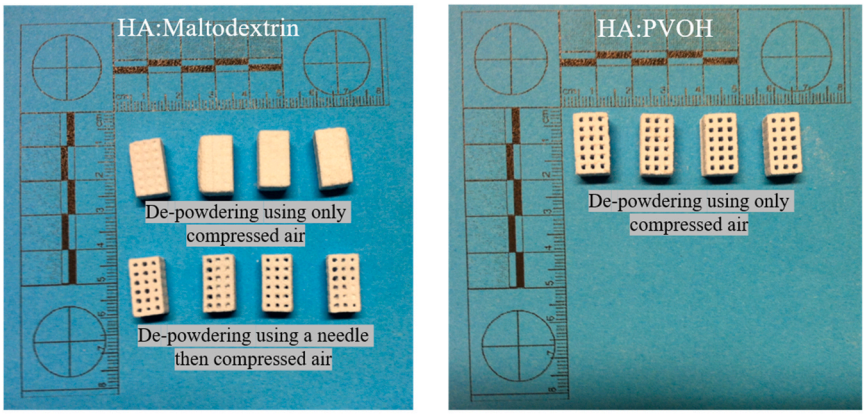

	10 wt.%	20 wt.%	30 wt.%
Maltodextrin			
PVOH (low MW)			
PVOH (high MW)			

Insufficient Strength Sufficient Strength

Fig. 5. Processing behaviour of HA powders mixed with maltodextrin, PVOH (low MW), and PVOH (high MW). After de-powdering, the difference in removing powders from the 3D printed scaffolds between HA:maltodextrin and HA:PVOH was demonstrated. Formulations that demonstrated sufficient handling strength post-printing were denoted by blue colour, and those exhibiting an insufficient handling strength were denoted by grey colour. (For interpretation of the references to color in this figure legend, the reader is referred to the web version of this article.)

from the HA: PVOH (low MW) powder blend exhibited the lowest compressive strength when compared the other powder blend formulations investigated. The compressive modulus data followed a similar trend to the compressive strength data except for the 3D printed scaffolds fabricated from the maltodextrin formulation, which exhibited the highest compressive modulus. Analysing the PVOH formulations, the 70:30 wt% HA:PVOH (high MW) demonstrated the highest compressive modulus of 88.96 ± 3.36 MPa. This result was $\geq 600\%$ higher than compressive modulus for the 3D printed scaffolds fabricated from the PVOH (low MW) formulation at the same powder ratio.

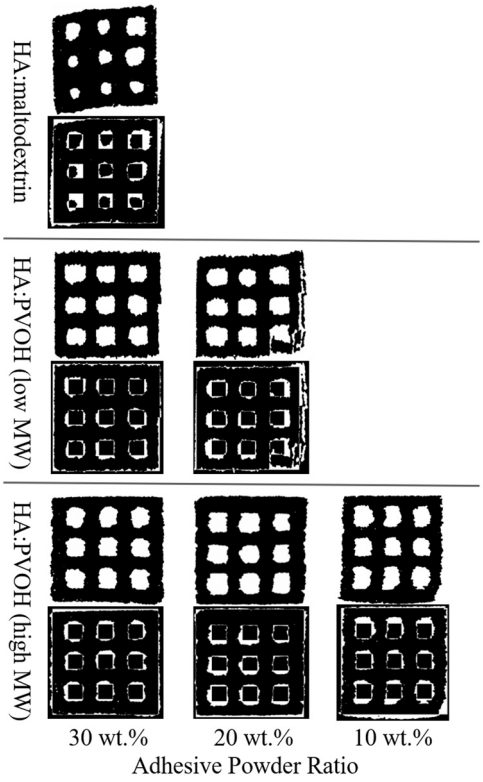

Fig. 6. Examples of the cross-sectional images obtained using μ-CT scanning of the AM scaffolds from different powder blend formulations. Each of the cross-sectional images was registered with the designed image, shown below the cross-sectional images.

4. Discussion

To the best of our knowledge, this is the first time that a water binder jetting AM formulation containing HA at a high level wt% content (≥ 70 wt%) achieving a high level of printability has been reported. Specifically, these powder formulations: (i) demonstrated a compressive strength approx. ≥ 500% higher than the commercial $CaSO_4$-based powder formulation; (ii) contained ≥ 70 wt% HA; (iii) exhibited good geometrical accuracy in the 3D structure and (iv) worked on a repeatable basis with standard water-based inks. The same 3D printed solid structure fabricated from 100% commercial $CaSO_4$-based powder exhibited a compressive strength of 1.10 MPa [20]. Blending 75 wt% commercial $CaSO_4$-based powder with 25 wt% HA increased the average compressive strength to 1.98 MPa [20]. However, in this study, 3D scaffolds demonstrating a significantly higher compressive strength (i.e. 5.63 MPa) by incorporating ≤ 30 wt% adhesive-based powders were fabricated. Incorporating a higher wt% HA content in the powder formulation has the potential to provide greater osteoconductivity for bone applications.

Nevertheless, it is crucial to select an adhesive powder with appropriate physical characteristics. For PVOH, the molecular weight plays an important role in determining the quality of the 3D printed scaffold. In general, an increase in the degree of polymerisation has been reported to result in higher solution viscosity and greater tensile strength of the polymer membrane [43,44]. These characteristics are particularly favourable considering that PVOH was acting as a binding adhesive for the HA particles. PVOH with higher solution viscosity can potentially offer greater stability during binder jetting AM process. Following water evaporation, a high-strength 3D printed scaffold bound by a PVOH membrane resulted, which was demonstrated from the compressive data, i.e. the high MW PVOH grade of adhesive powder was superior when compared to the low MW equivalent. Even, using PVOH (high MW) at 10 wt% resulted in significantly higher compressive properties when compared to 30 wt% PVOH (low MW) (p-value < 0.05). The major advantage of using PVOH (high MW) as the binding adhesive allows for the use of a higher HA content in the powder formulation. Both the PVOH grades (high MW and low MW) at 30 wt% demonstrated similar geometrical accuracy, wetting ratio and droplet penetration behaviour. The only difference was observed for the 3D printed scaffold fabricated from the HA:PVOH (low MW) powder formulation, which demonstrated poor mechanical properties and in part was caused by structural damage and poor handling properties at 20 wt% and 10 wt% PVOH content, respectively.

The other adhesive investigated was a maltodextrin-based material, which demonstrated a molecular weight distribution close to the PVOH (high MW) and exhibited a reaction similar to the water ink in a dissolution-precipitation mechanism. However, the quality of the 3D scaffolds fabricated using the HA:maltodextrin powder formulation was distinct. The major issue with using maltodextrin as the adhesive with the HA was excessive wetting, which caused difficulties in de-powdering and poor geometrical accuracy. The excessive wetting of maltodextrin affected powders in the unbound areas within the scaffold structure and

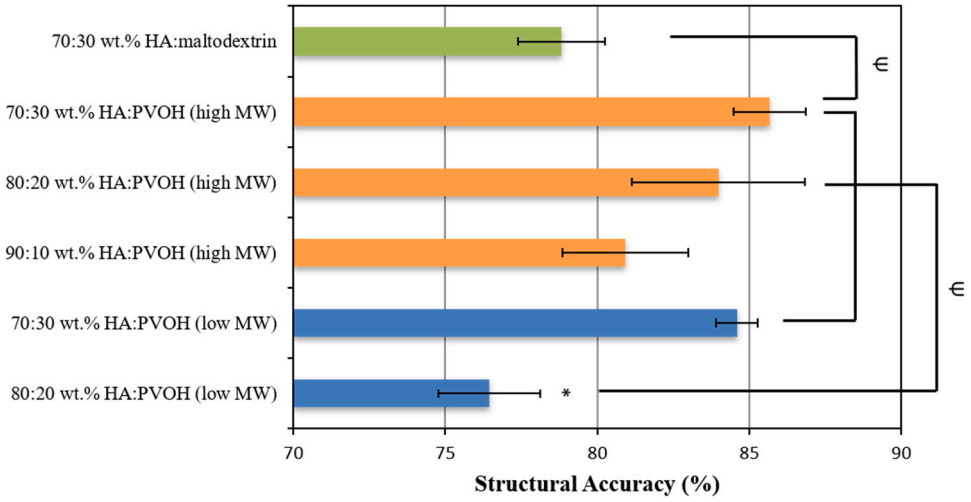

Fig. 7. Mean structural accuracy ± SD (%) of AM 3D porous scaffolds printed from powder blend formulations of various adhesives at differing ratios. * Denotes p-value < 0.05, indicating a significant difference between powders having differing HA:adhesive ratios. Ψ denotes p-value < 0.05, indicating a significant difference between powders consisting of differing binding adhesives.

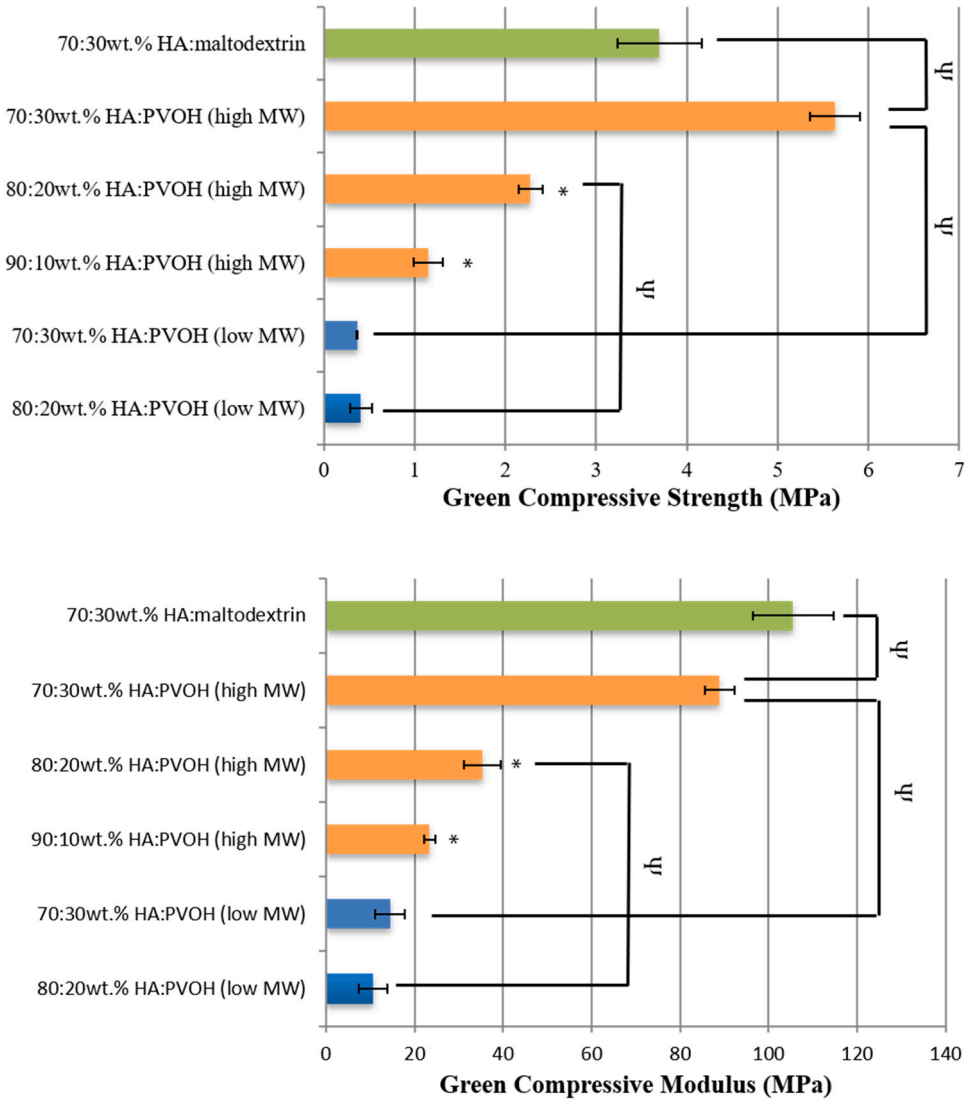

Fig. 8. Mean green compressive strength and compressive modulus ± SD (MPa) of AM 3D printed solid printed from powder blend formulations consisting of various adhesives at differing ratios. * Denotes p-value < 0.05, indicating a significant difference between powders having differing HA:adhesive ratios. Ψ denotes p-value < 0.05, indicating a significant difference between powders consisting of differing binding adhesives.

a needle was required to remove the unbound powder from the 3D printed scaffold. This was a significant issue since the use of needle potentially damaged the structural integrity of the 3D printed scaffold. The greater penetration depth and wetting ratio data for also confirmed the excessive wetting of water-based ink with HA:maltodextrin powder. At the same compositional ratio (30 wt%), maltodextrin wetted the surrounding HA powder more than four times higher when compared to the PVOH (Fig. 4). The excessive wetting also resulted in distorted shapes and non-uniform sizes of the 3D printed scaffolds fabricated from HA:maltodextrin. The majority of struts within the structure were larger than the size defined in the initial CAD design. This wetting behaviour negatively influenced the geometrical accuracy of the printed scaffolds, which restricted the control and prediction of their respective performance. The HA:maltodextrin at 30 wt% adhesive ratio showed good compressive properties. However, it was not contributed by the intrinsic material properties, but simply due to a greater degree of wetting within the structure. This was proved when maltodextrin was mixed at lower ratios, the HA:maltodextrin structures did not possess sufficient strength for handling during post-fabrication. It is postulated that this was because PVOH exhibited better intrinsic mechanical properties than maltodextrin. Natural polymers such as maltodextrin are excellent in biological responses with self-degradable moieties but generally weak under mechanical loading due to their relatively weak chemical bonding [45–47]. Maltodextrin is basically a collection of glucose units held together by glycosidic bonds [45]. For example, a previous study reported, a HA-maltodextrin structure exhibited a green strength of 0.7 MPa, which is significantly lower than the minimum requirements for cancellous bone regeneration [18]. Therefore, maltodextrin has been used mainly to improve the biological performances of the bioceramics in bone tissue engineering [48,49]. Contrarily, synthetic polymers have weaker biological responses but better mechanical properties. PVOH is one of the mostly investigated polymers to improve the strength and toughness of bioceramics due to its capability to build strong binding to the surrounding ceramics [50–52]. This study also demonstrated PVOH provided better mechanical improvement to HA compared to maltodextrin.

This study has demonstrated the importance of using the droplet penetration method to understand the relationship (and the interaction thereof) between the powder bed and water-based ink during the binder jetting AM process. The HA:adhesive powder formulations investigated in this study showed very rapid droplet penetration time (< 400 ms), which demonstrated good efficiency in absorbing the ink droplets. Due

to this rapid penetration time, the powder wettability did not reach equilibrium before the droplet fully penetrated the surface of the powder bed. Therefore, it was difficult to characterise the wetting angle of the powder, which is often useful to infer the surface roughness, surface energy and hydrophilicity of the powder bed [53]. The rapid penetration occurred due to the increased hydrophobicity of the powder compositions after mixing with the water-soluble adhesives. A previous study used $CaSO_4$ as the adhesive powder for HA but only managed to reach an average penetration time of 1500 ms [20]. A faster droplet penetration time leads to faster ink-powder interaction, which is beneficial for AM manufacturing considering the structure of the 3D printed scaffold is built voxel by voxel.

In summary, a high MW grade of PVOH is the best candidate as the adhesive powder for HA when the binder jetting AM process is being considered. PVOH is a non-toxic biopolymer that can potentially form a promising bioceramic-polymer composite to mimic the natural bone. The biopolymer component demonstrates good toughness, which provides balance to the intrinsic brittle nature of the HA [54]. This study successfully established HA-based powder formulations that potentially provide great structural, mechanical and biological properties of the binder jetting AM manufactured scaffolds. This first step achievement is often critical to the eventual success in developing new bone substitutes for bone tissue engineering applications.

5. Future perspective

In general, ceramic structures manufactured using binder jetting AM have low mechanical properties [9,12,14]. For example, the commercial binder-jetting powder demonstrated a green strength of 1.10 MPa. Consequently, various post-processing approaches such as sintering [21] and polymer infiltration [9] were adopted to improve the mechanical properties. Nevertheless, the greatest improvement achieved in this study was a significant increase in green strength (5.63 MPa) owing to the development of novel powder compositions (i.e. 30:70 PVOH:HA). It was more than 500% higher than that of the commercial powder. Most importantly, this is now in the mid-range of natural cancellous bone (2–12 MPa) [55]. Considering the proposed application is targeted towards non-load bearing bone implants, the developed composition has sufficiently high mechanical properties that can essentially eliminate the need to adopt post-processing method. Additionally, sintering will inevitably remove the PVOH from the structure, which is not ideal from a tissue engineering perspective. In the biomaterial research field, ceramic/polymer composites have been the trend for development of bone tissue implants due to their resemblance with organic/inorganic phases in natural bone composition [56–58]. It combines the merits of each component, i.e. the ceramic phase provides osteoconductivity and the polymer phases demonstrates appropriate toughness [56]. This study has essentially printed HA particles within a PVOH matrix. This follows the biomimetic concept that in bone structure, HA particles are dispersed within a polymer-based matrix (i.e. collagen) [59]. An adverse effect would result if the polymer-based material was removed due to sintering and only the ceramic remained. Due to the abovementioned reasons, the authors would like to propose the use of as-printed scaffolds developed in this study directly for potential non-load bearing bone tissue applications, without post-processing treatment.

Following this work, further investigation on this PVOH:HA composition is proposed to determine the bioresorption and bioresponsiveness of the scaffold structures. It would be interesting to evaluate the effects of a secondary phase of PVOH on the bioresorption behaviour of a principal HA material. A dynamic flow reactor to mimic body fluid circulation would be preferred for conducting the bioresorption characterisation. A dynamic flow reactor can create continuous flow that replicates how the scaffold structure would degrade or resorb in vivo. A previous study found a dynamic flow reactor is a particularly useful tool to characterise scaffolds manufactured using binder jetting AM [21]. Going forward, it also important to understand how efficient the 3D printed PVOH matrix can bind the HA particles. A good indication of particle removal is water absorption of the PVOH:HA scaffolds, which increases with more water uptake within structural flaws [21]. Understanding the surface hydrophilicity or wettability is also recommended to characterise change in the PVOH/HA ratio during resorption. The resorption rate should coincide with the bone tissue growth rate and bone remodelling, which will vary considerably based on the type and position of bone to be repaired [60]. The bioresponsiveness of the PVOH:HA scaffold is also important for understanding its biocompatibility and osteoconductive properties. Cell viability, proliferation differentiation rates should be characterised using appropriate in vitro studies and in vivo small and large animal models. The PVOH:HA scaffold will only prove to be useful for triggering bone repair and regeneration if collective information shows positive results within these in vitro and in vivo studies. The specific application of the described PVOH:HA-based scaffold should be determined following studies to understand the bioresorption and bioresponsiveness behaviour. The proposed experiments relate to the design and evaluation of PVOH:HA 3D printed scaffolds specifically towards potential clinical application. The scale and scope of this work are beyond this current study, which focused on the formulation and processing development of the PVOH:HA 3D printed scaffolds.

6. Conclusions

This is the first study to demonstrate a high level of printability when using a formulation containing $\geq$ 70 wt% HA powder and a water-based binder in the binder jetting AM process. Specifically, we developed HA: adhesive powder formulations demonstrating greater 3D printability using the binder jetting AM process when compared to the literature [17–23]. High geometrical accuracy ($>$ 85%) and excellent green compressive strength (5.63 $\pm$ 0.27 MPa) were achieved when high MW PVOH powder (30 wt%) was blended with HA. This study also investigated the fundamental droplet penetration behaviour in different powder formulations. From these studies, it was observed that the maltodextrin-based adhesive exhibited excessive wetting when used in conjunction with the water-based ink – thereby causing poor geometrical accuracy and difficulty in removing unbound powder from within the structure of the 3D printed scaffold. Additionally, the low MW grade of PVOH resulted in a 3D printed scaffold demonstrating poorer compressive properties. In summary, adoption of the proposed optimal powder formulation with a water-based binder significantly improved the printability of HA-based 3D scaffolds manufactured using the binder jetting AM process, which can potentially improve their mechanical, structural and biological performances for bone tissue engineering applications.

CRediT authorship contribution statement

Zuoxin Zhou: Conceptualization, Methodology, Investigation, Formal analysis, Writing - original draft. **Alex Lennon:** Visualization. **Fraser Buchanan:** Supervision, Writing - review & editing. **Helen O. McCarthy:** Visualization, Writing - review & editing. **Nicholas Dunne:** Conceptualization, Supervision, Writing - review & editing, Project administration.

Declaration of Competing Interest

The authors declare that they have no known competing financial interests or personal relationships that could have appeared to influence the work reported in this paper.

Acknowledgements

The authors thank the School of Mechanical and Aerospace Engineering from Queen's University Belfast, United Kingdom to provide

International Studentship that has been used to support this work.

References

[1] R.Z. Legeros, R.G. Craig, Strategies to affect bone remodeling: osteointegration, J. Bone Miner. Res. 8 (S2) (1993) S583–S596.

[2] J.P. Schmitz, J.O. Hollinger, S.B. Milam, Reconstruction of bone using calcium phosphate bone cements: a critical review, J. Oral Maxillofac. Surg. 57 (9) (1999) 1122–1126.

[3] C.J. Damien, J.R. Parsons, Bone graft and bone graft substitutes: a review of current technology and applications, J. Appl. Biomater. 2 (3) (1991) 187–208.

[4] J.C. Park, H.C. Lim, J.Y. Sohn, J.H. Yun, U.W. Jung, C.S. Kim, K.S. Cho, C.K. Kim, S. H. Choi, Bone regeneration capacity of two different macroporous biphasic calcium materials in rabbit calvarial defect, J. Korean Acad. Periodontol. Suppl. 39 (2009) 223–230.

[5] S.D. Cook, Hydroxyapatite-coated total hip replacement, Dent. Clin. N. Am. 36 (1) (1992) 235–238.

[6] C.D. Friedman, P.D. Costantino, C.H. Snyderman, L.C. Chow, S. Takagi, Reconstruction of the frontal sinus and frontofacial skeleton with hydroxyapatite cement, Arch. Facial Plast. Surg. 2 (2) (2000) 124–129.

[7] M. Hallman, M. Hedin, L. Sennerby, S. Lundgren, A prospective 1-year clinical and radiographic study of implants placed after maxillary sinus floor augmentation with bovine hydroxyapatite and autogenous bone, J. Oral Maxillofac. Surg. 60 (3) (2002) 277–284.

[8] Z. Zhou, C.A. Mitchell, F.J. Buchanan, N.J. Dunne, Effects of heat treatment on the mechanical and degradation properties of 3D-printed calcium-sulphate-based scaffolds, ISRN Biomater. 2013 (2012).

[9] Z. Zhou, E. Cunningham, A. Lennon, H.O. McCarthy, F. Buchanan, S.A. Clarke, N. Dunne, Effects of poly (ε-caprolactone) coating on the properties of three-dimensional printed porous structures, J. Mech. Behav. Biomed. Mater. 70 (2017) 68–83.

[10] E. Vorndran, M. Klarner, U. Klammert, L.M. Grover, S. Patel, J.E. Barralet, U. Gbureck, 3D powder printing of β-tricalcium phosphate ceramics using different strategies, Adv. Eng. Mater. 10 (12) (2008) B67–B71.

[11] C. Bergmann, M. Lindner, W. Zhang, K. Koczur, A. Kirsten, R. Telle, H. Fischer, 3D printing of bone substitute implants using calcium phosphate and bioactive glasses, J. Eur. Ceram. Soc. 30 (12) (2010) 2563–2567.

[12] S. Bose, S. Vahabzadeh, A. Bandyopadhyay, Bone tissue engineering using 3D printing, Mater. Today 16 (12) (2013) 496–504.

[13] G. Brunello, S. Sivolella, R. Meneghello, L. Ferroni, C. Gardin, A. Piattelli, B. Zavan, E. Bressan, Powder-based 3D printing for bone tissue engineering, Biotechnol. Adv. 34 (5) (2016) 740–753.

[14] A. Butscher, M. Bohner, S. Hofmann, L. Gauckler, R. Müller, Structural and material approaches to bone tissue engineering in powder-based three-dimensional printing, Acta Biomater. 7 (3) (2011) 907–920.

[15] J.H. Lim, K. Kuk, S.J. Shin, S.S. Baek, Y.J. Kim, J.W. Shin, Y.S. Oh, Failure mechanisms in thermal inkjet printhead analyzed by experiments and numerical simulation, Microelectron. Reliab. 45 (3–4) (2005) 473–478.

[16] G.D. Martin, S.D. Hoath, I.M. Hutchings, Inkjet printing-the physics of manipulating liquid jets and drops, J. Phys. Conf. Ser. 105 (1) (2008) 012001. IOP Publishing.

[17] J. Will, R. Melcher, C. Treul, N. Travitzky, U. Kneser, E. Polykandriotis, R. Horch, P. Greil, Porous ceramic bone scaffolds for vascularized bone tissue regeneration, J. Mater. Sci. Mater. Med. 19 (8) (2008) 2781–2790.

[18] R. Chumnanklang, T. Panyathanmaporn, K. Sitthiseripratip, J. Suwanprateeb, 3D printing of hydroxyapatite: effect of binder concentration in pre-coated particle on part strength, Mater. Sci. Eng. C 27 (4) (2007) 914–921.

[19] J. Suwanprateeb, R. Sanngam, W. Suvannapruk, T. Panyathanmaporn, Mechanical and in vitro performance of apatite–wollastonite glass ceramic reinforced hydroxyapatite composite fabricated by 3D-printing, J. Mater. Sci. Mater. Med. 20 (6) (2009) 1281.

[20] Z. Zhou, F. Buchanan, C. Mitchell, N. Dunne, Printability of calcium phosphate: calcium sulfate powders for the application of tissue engineered bone scaffolds using the 3D printing technique, Mater. Sci. Eng. C 38 (2014) 1–10.

[21] Z. Zhou, E. Cunningham, A. Lennon, H.O. McCarthy, F. Buchanan, N. Dunne, Development of three-dimensional printing polymer-ceramic scaffolds with enhanced compressive properties and tuneable resorption, Mater. Sci. Eng. C 93 (2018) 975–986.

[22] W. Chai, Q. Wei, M. Yang, K. Ji, Y. Guo, S. Wei, Y. Wang, The printability of three water based polymeric binders and their effects on the properties of 3D printed hydroxyapatite bone scaffold, Ceram. Int. 46 (5) (2020) 6663–6671.

[23] R. Chumnanklang, T. Panyathanmaporn, K. Sitthiseripratip, J. Suwanprateeb, 3D printing of hydroxyapatite: effect of binder concentration in pre-coated particle on part strength, Mater. Sci. Eng. C 27 (4) (2007) 914–921.

[24] Y. Shanjani, J.A. De Croos, R.M. Pilliar, R.A. Kandel, E. Toyserkani, Solid freeform fabrication and characterization of porous calcium polyphosphate structures for tissue engineering purposes, J. Biomed. Mater. Res. Part B Appl. Biomater. 93 (2) (2010) 510–519.

[25] R. Trombetta, J.A. Inzana, E.M. Schwarz, S.L. Kates, H.A. Awad, 3D printing of calcium phosphate ceramics for bone tissue engineering and drug delivery, Ann. Biomed. Eng. 45 (1) (2017) 23–44.

[26] B.K. Tay, V.V. Patel, D.S. Bradford, Calcium sulfate- and calcium phosphate-based bone substitutes. Mimicry of the mineral phase of bone, Orthop. Clin. N. Am. 30 (4) (1999) 615–623.

[27] M. Nilsson, E. Fernandez, S. Sarda, L. Lidgren, J. Planell, Characterization of a novel calcium phosphate/sulphate bone cement, J. Biomed. Mater. Res. 61 (4) (2002) 600–607.

[28] Y. Shanjani, J.A. DeCroos, R.M. Pilliar, R.A. Kandel, E. Toyserkani, Solid freeform fabrication and characterization of porous calcium polyphosphate structures for tissue engineering purposes, J. Biomed. Mater. Res. Part B Appl. Biomater. 93 (2) (2010) 510–519.

[29] V. Goodship, D.K. Jacobs. Polyvinyl Alcohol: Materials, Processing and Applications 12, Vol. 16, Smithers Rapra Technology, 2009.

[30] Z. Zhou, I. Salaoru, P. Morris, G.J. Gibbons, Additive manufacturing of heat-sensitive polymer melt using a pellet-fed material extrusion, Addit. Manuf. 24 (2018) 552–559.

[31] Z. Gurturk, A. Tezcaner, A.D. Dalgic, S. Korkmaz, D. Keskin, Maltodextrin modified liposomes for drug delivery through the blood–brain barrier, RSC Med. Chem. R. Soc. Chem. (2017) 1337–1345.

[32] M.I. Baker, S.P. Walsh, Z. Schwartz, B.D. Boyan, A review of polyvinyl alcohol and its uses in cartilage and orthopedic applications, J. Biomed. Mater. Res. Part B Appl. Biomater. 100 (5) (2012) 1451–1457.

[33] N. Alexandre, J. Ribeiro, A. Gärtner, T. Pereira, I. Amorim, J. Fragoso, A. Lopes, J. Fernandes, E. Costa, A. Santos-Silva, M. Rodrigues, Biocompatibility and hemocompatibility of polyvinyl alcohol hydrogel used for vascular grafting—in vitro and in vivo studies, J. Biomed. Mater. Res. Part A 102 (12) (2014) 4262–4275.

[34] C.M. Hassan, N.A. Peppas, Structure and applications of poly (vinyl alcohol) hydrogels produced by conventional crosslinking or by freezing/thawing methods. Biopolymers: PVA Hydrogels, Anionic Polymerisation Nanocomposites, Springer, Berlin, Heidelberg, 2000, pp. 37–65.

[35] N. Dunne, J. Hill, P. Mcafee, K. Todd, R. Kirkpatrick, M. Tunney, S. Patrick, In vitro study of the efficacy of acrylic bone cement loaded with supplementary amounts of gentamicin: effect on mechanical properties, antibiotic release, and biofilm formation, Acta Orthop. 78 (6) (2007) 774–785.

[36] J. Hill, J. Orr, N. Dunne, In vitro study investigating the mechanical properties of acrylic bone cement containing calcium carbonate nanoparticles, J. Mater. Sci. Mater. Med. 19 (11) (2008) 3327–3333.

[37] J.M. Fitzpatrick, D.L. Hill, C.R. Maurer, Image registration, in: Handbook of Medical Imaging, 2000, pp. 447–513.

[38] B. Zitova, J. Flusser, Image registration methods: a survey, Image Vis. Comput. 21 (11) (2003) 977–1000.

[39] A.A. Goshtasby, 2-D and 3-D Image Registration: for Medical, Remote Sensing, and Industrial Applications, John Wiley & Sons, 2005.

[40] C.A. Schneider, W.S. Rasband, K.W. Eliceiri, NIH Image to ImageJ: 25 years of image analysis, Nat. Methods 9 (7) (2012) 671–675.

[41] D.G. Lowe, Distinctive image features from scale-invariant keypoints, Int. J. Comput. Vis. 60 (2) (2004) 91–110.

[42] P.E. Slade (Ed.), Polymer Molecular Weights, Part 2 Vol. 4, CRC Press, 1975.

[43] G.O. Yahya, S.A. Ali, M.A. Al-Naafa, E.Z. Hamad, Preparation and viscosity behavior of hydrophobically modified poly (vinyl alcohol)(PVA), J. Appl. Polym. Sci. 57 (3) (1995) 343–352.

[44] Z. Zhifeng, Q. Kun, Effects of the molecular structure of polyvinyl alcohol on the adhesion to fibre substrates, Fibres Text. East. Eur. 15 (1) (2007) 82.

[45] B.C. Simionescu, D. Ivanov, Natural and synthetic polymers for designing composite materials, in: Handbook of Bioceramics and Biocomposites, 2016, pp. 233–286.

[46] S. Bhatia, Natural polymers vs synthetic polymer. Natural Polymer Drug Delivery Systems, Springer, Cham, 2016, pp. 95–118.

[47] F. Donnaloja, E. Jacchetti, M. Soncini, M.T. Raimondi, Natural and synthetic polymers for bone scaffolds optimization, Polymers 12 (4) (2020) 905.

[48] B.T. Phan, H.T. Nguyen, H.Q. Đao, L.V. Pham, T.T. Quan, D.B. Nguyen, H. T. Nguyen, T.T. Vu, Synthesis and characterization of nano-hydroxyapatite in maltodextrin matrix, Appl. Nanosci. 7 (1–2) (2017) 1–7.

[49] A. Kumar, A.R. Akkineni, B. Basu, M. Gelinsky, Three-dimensional plotted hydroxyapatite scaffolds with predefined architecture: comparison of stabilization by alginate cross-linking versus sintering, J. Biomater. Appl. 30 (8) (2016) 1168–1181.

[50] C. Vitale-Brovarone, F. Baino, E. Verné, High strength bioactive glass-ceramic scaffolds for bone regeneration, J. Mater. Sci. Mater. Med. 20 (2) (2009) 643–653.

[51] S.K. Swain, S. Bhattacharyya, D. Sarkar, Fabrication of porous hydroxyapatite scaffold via polyethylene glycol-polyvinyl alcohol hydrogel state, Mater. Res. Bull. 64 (2015) 257–261.

[52] L. Stipniece, I. Narkevica, M. Sokolova, J. Locs, J. Ozolins, Novel scaffolds based on hydroxyapatite/poly (vinyl alcohol) nanocomposite coated porous TiO2 ceramics for bone tissue engineering, Ceram. Int. 42 (1) (2016) 1530–1537.

[53] A. Alghunaim, S. Kirdponpattara, B.M.Z. Newby, Techniques for determining contact angle and wettability of powders, Powder Technol. 287 (2016) 201–215.

[54] S. Pineda-Castillo, A. Bernal-Ballén, C. Bernal-López, H. Segura-Puello, D. Nieto-Mosquera, A. Villamil-Ballesteros, D. Muñoz-Forero, L. Munster, Synthesis and characterization of poly (vinyl alcohol)-chitosan-hydroxyapatite scaffolds: a promising alternative for bone tissue regeneration, Molecules 23 (10) (2018) 2414.

[55] D.R. Carter, W.C. Hayes, Bone compressive strength: the influence of density and strain rate, Science 194 (4270) (1976) 1174–1176.

[56] K. Rezwan, Q.Z. Chen, J.J. Blaker, A.R. Boccaccini, Biodegradable and bioactive porous polymer/inorganic composite scaffolds for bone tissue engineering, Biomaterials 27 (18) (2006) 3413–3431.

[57] A.J.W. Johnson, B.A. Herschler, A review of the mechanical behavior of CaP and CaP/polymer composites for applications in bone replacement and repair, Acta Biomater. 7 (1) (2011) 16–30.

[58] H. Zhou, J.G. Lawrence, S.B. Bhaduri, Fabrication aspects of PLA-CaP/PLGA-CaP composites for orthopedic applications: a review, Acta Biomater. 8 (6) (2012) 1999–2016.

[59] S. Weiner, H.D. Wagner, The material bone: structure-mechanical function relations, Annu. Rev. Mater. Sci. 28 (1) (1998) 271–298.

[60] S. Bose, M. Roy, A. Bandyopadhyay, Recent advances in bone tissue engineering scaffolds, Trends Biotechnol. 30 (10) (2012) 546–554.